Optical Materials 125 (2022) 112075

Contents lists available at ScienceDirect

Optical Materials

journal homepage: www.elsevier.com/locate/optmat

Numerical modeling and performance optimization of carbon-based hole transport layer free perovskite solar cells

Ehsan Raza [a,b], Zubair Ahmad [b,c,*], Muhammad Asif [a], Fakhra Aziz [a], Kashif Riaz [d], Muhammad Qasim Mehmood [d], Jolly Bhadra [b,c], Noora J. Al-Thani [b]

[a] Department of Electronics, University of Peshawar, Peshawar, 25120, Pakistan
[b] Qatar University Young Scientists Center (QUYSC), Qatar University, 2713, Doha, Qatar
[c] Center for Advanced Materials (CAM), Qatar University, 2713, Doha, Qatar
[d] Department of Electrical Engineering, Information Technology University (ITU), 346-B, Ferozepur Road, Lahore, Pakistan

ARTICLE INFO

Keywords:
Perovskite solar cells
Device simulation
Triple cation perovskite
Carbon electrode
HTL-Free structure
The power conversion efficiency

ABSTRACT

Owing to low production cost and ease of processing, hole-transport layer (HTL) free carbon electrode-based perovskite solar cells (c-PSCs) have emerged as a potential photovoltaic (PV) technology. Despite this, c-PCSs still have to achieve the high photon conversion efficiency exhibited by standard PSCs using HTLs. In the present work, device modeling of $Cs_x(FA_{0.4}MA_{0.6})_{1-x}PbI_{2.8}Br_{0.2}$ based HTL-free c-PSC was presented using the simulation program Solar Cell Capacitance Simulator (SCAPS). Output results were successfully replicated in the simulation that were comparable to experimentally reported values. Furthermore, several parameters affecting device performance, such as the absorber layer, the electron transport layer (ETL), front contact thicknesses, and doping concentrations, are studied and optimized. Additionally, the defect density at the perovskite/ETL interface is investigated. Under optimized conditions, a high open-circuit voltage of 1.13 V, short-circuit current density of 22.54 mA/cm^2, fill factor of 79.75%, and photon conversion efficiency of 20.43% is achieved. Results demonstrate the promising features of the proposed HTL-free c-PSC. Lastly, the impact of temperature and work function of back metal contacts were also examined. The simulation results suggest a direction to design low-cost and highly efficient HTL-free c-PSCs.

1. Introduction

In recent years, the scientific community has shown a significant research interest in perovskite solar cells (PSCs) owing to their cost-effectiveness and high performance. The key features attributed to PSCs include light absorption through a broad-spectrum range [1], direct and tunable bandgap [2], long charge carriers diffusion lengths [3], and excellent carrier mobilities [4]. Thanks to their remarkable features, the efficiency values upsurged from 3.8% [5] to a decent value of over 25% [6], beating the maximum efficiency of copper indium gallium selenide (CIGS) and achieving one of the crystalline-silicon solar cells.

Most highly efficient PSCs employ organic hole transport layers (HTLs) and back metal electrodes such as silver or gold [7,8]. However, instability issues caused by organic HTLs and higher fabrication costs associated with back metal contacts hinder the viability of PSCs towards entry into the photovoltaic (PV) market [9]. The PSCs have evolved through the mesoporous configuration [10], the planar configuration [11], the hole transport layer free configuration [12], and electron transport layer free configuration [13]. Interestingly, owing to the perovskite distinctive ambipolar nature, it was revealed that HTL-free PSCs may also perform well [14]. Therefore, tremendous research efforts have been dedicated to design stable and cost-effective HTL-free PSCs in recent years.

To date, a few HTL-free PSCs structures have been reported [15–18]. Among those, carbon-based PSCs (c-PSCs) are considered the potential contenders for highly stable, cost-effective, and large-scale solutions processed PSCs [19]. In 2013, the first report on c-PSC was presented with an efficiency of 6.6% [20]. A year later, a 12.8% efficiency was reported by Mei et al. [12] with improved stability. So far, the highest reported power conversion efficiency (PCE) values of 15.9% [21] and 14.88% [14] have been reported by c-PSCs based on $MAPbI_3$ and $FAMAPbI_3$ compounds, respectively. However, degradation issues in $MAPbI_3$ under thermal and moisture conditions and phase instability in

* Corresponding author. Center for Advanced Materials (CAM), Qatar University, 2713, Doha, Qatar.
E-mail address: zubairtarar@qu.edu.qa (Z. Ahmad).

https://doi.org/10.1016/j.optmat.2022.112075
Received 6 November 2021; Received in revised form 25 January 2022; Accepted 2 February 2022
Available online 9 February 2022

$FAPbI_3$ restrict their applications in high-performance PSCs [22,23].

It was revealed that the incorporation of cesium (Cs) with formamidinium (FA) or methylammonium (MA) could enhance the stability and performance of PSCs [23]. In our previous report, we employed Cs/FA/MA triple cation perovskite composition in HTL-free c-PSC and reported 13.3% efficiency [24]. In 2017, Liu et al. [14] have developed a fully printable c-PSC by incorporating $Cs_x(FA_{0.4}MA_{0.6})_{1-x}PbI_{2.8}Br_{0.2}$ along with metal oxides mesoporous TiO_2/Al_2O_3/-NiO (PIN) layer. They demonstrated 17.02% efficiency with 1000 h of device stability. This is the record maximum PCE value ever achieved in c-PSC structures. This demonstrates the potential of Cs-based triple cation perovskite composition towards highly efficient and stable PSCs. However, the PCE values in HTL-free structures are lagging than their counterparts with HTLs. This motivates us to investigate, optimize our experimentally reported c-PSC device structure with 13.39% PCE using $Cs_x(FA_{0.4}MA_{0.6})_{1-x}PbI_{2.8}Br_{0.2}$ absorber layer and enhance its performance further [24].

In addition, a small number of efforts based on simulation work have been reported on HTL-free c-PSCs. For instance, 14.7% efficiency was reported by Rai et al. [25] with uniform doping. Lin and co-workers demonstrated efficiency values of 25.07% and 25.15% by employing n and p-type perovskite homojunction and gradient doping, respectively [26,27]. It is worth mentioning that in this work, we show a realistic and experimentally achievable approach to develop HTL-free c-PSCs, as well as showing that uniform doping can achieve over 20% efficiency.

2. Device modeling and input parameters

In the present study, the $Cs_x(FA_{0.4}MA_{0.6})_{1-x}PbI_{2.8}Br_{0.2}$ as an active absorber layer was employed in HTL-free c-PSC configuration. The simulation program solar cell capacitance simulator (SCAPS, ver. 3.3.07) was used to model and optimize the experimentally reported HTL-free c-PSC. The software was developed by the research team at the Department of Electronics and Information Systems (ELIS), University of Gent, Belgium [28]. It solves three fundamental equations: Poisson and continuity equations for electrons and holes.

The HTL-free device configuration, as shown in Fig. 1a, is based on TCO/ETL/interface defect layer (IDL)/absorber layer/back metal contact. Here, TCO is for fluorine-doped tin oxide (FTO), ETL is for titanium dioxide (TiO_2), the absorber layer is $Cs_x(MA_{0.17}FA_{0.83})_{1-x}Pb(I_{0.83}Br_{0.17})_3$, and back metal contact is carbon (C). The IDL is assumed to consider the interface recombination. The energy band diagram is shown in Fig. 1b.

Parameters such as variation in thickness of the absorber layer, TiO_2, and FTO have been optimized to enhance device performance. Likewise, doping concentrations of the absorber, TiO_2, and FTO were changed, and their impact on device performance was investigated. In addition, the absorber defect density and interface quality at perovskite/TiO_2 are also analyzed. Lastly, the impact of operating temperature and work function of back metal was investigated.

The device input parameters for the various layers used in this study are presented in Table 1. The thickness of each layer and basic input parameters are extracted from different literatures, including experimental work [24,26,29–31]. Here, E_g denotes bandgap energy, χ represents electron affinity, εr shows relative permittivity, N_C is the effective density of states for conduction band, N_V is the effective density of states for valence band, μ_n is the mobility of electron, μ_p is the mobility of hole, N_A is the acceptor density and N_D represents donor density, and N_t represents defect density. Additional device parameters not defined in Table 1 are discussed as: Defect type is neutral with energy level as the center of E_g. Capture cross-section for electron and hole is 2.0×10^{14} cm^2. The energetic distribution is Gaussian, having

Table 1
Device Input parameters used in this simulation.

Parameters	FTO	TiO_2	IDL	Perovskite
Thickness (nm)	500 (Variable)	25 (Variable)	10	430 (Variable)
E_g (eV)	3.5	3.2	1.60	1.60
χ (eV)	4	4	3.9	3.9
ε_r	9	10	6.5	6.5
N_c (cm^{-3})	2.2×10^{18}	1.0×10^{21}	1.0×10^{17}	1.0×10^{17}
N_v (cm^{-3})	1.8×10^{19}	2.0×10^{20}	1.0×10^{17}	1.0×10^{17}
μ_n (cm^2/vs)	20	20	2.0	2.0
μ_p (cm^2/vs)	10	10	2.0	2.0
N_A (cm^{-3})	0	–	1.0×10^{13}	1.0×10^{13} (Variable)
N_D (cm^{-3})	2.0×10^{19} (Variable)	5.0×10^{19} (Variable)	0	0
N_t (cm^{-3})	1.0×10^{16}	1.0×10^{16}	1.0×10^{16}	2.60×10^{13} (Variable)
Reference	[32]	[26]	[24,29,30]	[24,29–31]

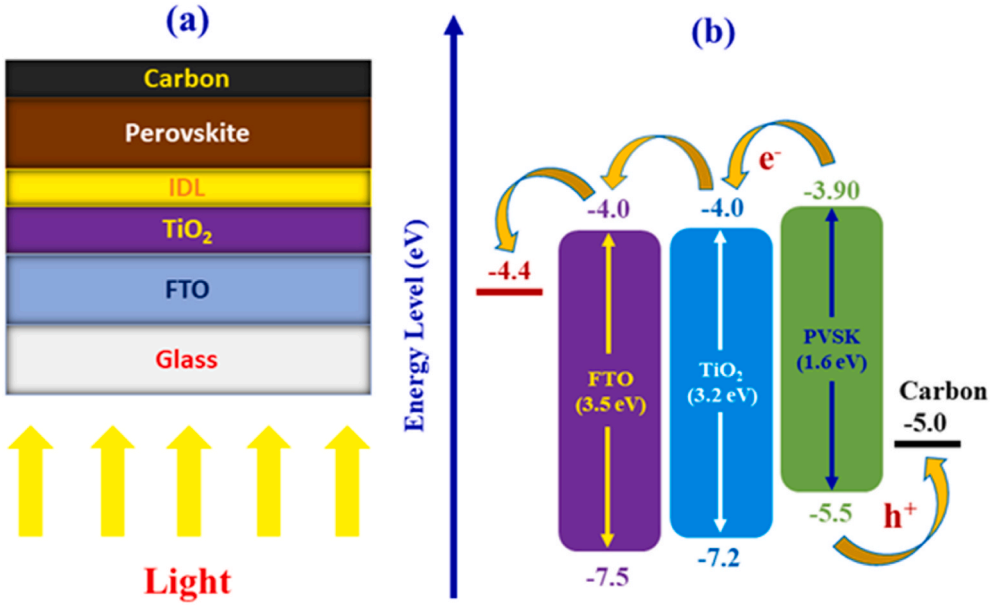

Fig. 1. (a) Device schematic of HTL-free carbon-based PSC (b) energy band diagram of c-PSC.

characteristic energy of 0.1 eV. The thermal velocity for electron and hole is 1.0×10^7 cm s^{-1}. For the carbon layer back electrode, 5.0 eV is used as the work function. For new materials, precise values of the device physical parameters are challenging to retrieve. Here, we gathered and considered them to the best of our understanding. The simulation study was carried out under the illumination with standard AM 1.5G spectrum.

3. Results and discussion

3.1. Simulation results validation

To validate our simulation model measurements, we designed the HTL-free structure in SCAPS and compared the results with experimentally reported FTO/TiO_2/$CsFAMAPbI_3$/C configuration [24,29]. Fig. 2a presents the J-V curves of experimental and simulated values, while the energy level diagram of the simulated device is illustrated in Fig. 2b. Table 2 provides a detailed comparison of J-V parameters. Our simulated results are pretty well with the experimentally reported values [24]. Thus, it confirms the reliability and validity of the present simulation study and suggests that the modeling parameters listed in Table 1 are comparable to realistic values.

3.2. Absorber layer thickness variation effect

The perovskite absorber layer is vitally essential to the PSC performance, as charge carriers are generated at this layer. Increasing the absorber layer thickness may result in charge carrier recombination before approaching the electrodes, whereas decreasing the absorber layer thickness will result in ineffective absorption of incident radiation. Consequently, the overall device performance will be reduced. Therefore, optimizing the absorber layer thickness is critical for an efficient PSC. Fig. 3a depicts variation in J-V curves as the absorber thickness changes from 100 to 1000 nm. Results indicate that the Jsc and Voc are improving with an optimization in the thickness of the absorber. As absorber thickness increases, many electron-hole pairs are generated, resulting in improved Jsc and Voc values. External quantum efficiency (EQE) describes the extent to which a solar cell can accumulate charge carriers from photons energy. Fig. 3b presents the spectral response of the HTL-free structure relative to wavelength with absorber thickness varying from 100 to 1000 nm. Results reveal that as absorber thickness decreases, photon absorption at longer wavelengths decreases. Because there are lesser photo-induced electron-hole pairs generation within the absorber layer. Furthermore, at wavelengths greater than 780 nm, EQE drops to zero because of inefficient light absorption below bandgaps at longer wavelengths with low energy.

Fig. 3c shows that the absorber layer thickness significantly affects the J-V parameters. The Jsc value increases from 13.81 mA/cm^2 to 22.62 mA/cm^2 as the absorber layer thickness increases from 100 to 600 nm. Beyond 600 nm absorber thickness, the Jsc grows slowly and saturates to 23 mA/cm^2. The growing behavior of Jsc is attributed to the increased number of long-wavelength light absorption resulting in enhanced charge carrier generation. At a small absorber thickness, the small number of long-wavelength photons are absorbed resulted in low charge carrier generation and hence the low value of Jsc. The Voc also increases from 0.84 to 0.91 V by increasing the absorber layer thickness up to 600 nm. Beyond that, it saturates at 0.91 V. It could be correlated with the high electron-hole pairs generation with increased light absorption and smaller absorber layer thickness. However, as thickness increases, the recombination rate increases, that affects Voc. In contrast to Jsc and Voc values, the FF value decreases drastically with increased absorber thickness. The increased thickness of the absorber causes high series resistance resulting in a decrease in FF. With absorber thickness ranging from 100 to 400 nm, PCE value increases from 8.68% to 13.15%. Beyond 400 nm, the PCE becomes saturated at 13%. Our simulation results present that the 700–800 nm thick absorber layer is suitable for high-performance HTL free c-PSCs. We performed further optimization of our simulated device by considering an 800 nm thick absorber layer. Additionally, the optical absorption coefficients graphs of all the layers are plotted and shown in Fig. S1.

3.3. Absorber doping concentration (N_A) and defect density (N_t) variation effect

The doping process has a substantial influence on the performance of semiconducting devices. In the present section, the absorber acceptor doping density (N_A) is varied, and its effect on the PV parameters is investigated. The N_A values have been changed from 10^{13} to 10^{17} cm^{-3}, and obtained results are illustrated in Fig. 4a. The results reveal that all Voc, FF, and PCE vary as the N_A value increases. The Jsc remains constant up to 10^{15} cm^{-3}, and then a decreasing behavior is observed from 10^{15} to 10^{17} cm^{-3}. This decrease in Jsc value is attributed to Auger recombination that dominates at higher doping concentration levels causes low device performance [30]. Results also show that Voc improves significantly up to 10^{17} cm^{-3}. However, up to 10^{16} cm^{-3}, the increase in Voc causes the improvement in FF and PCE. Whereas, beyond 10^{16} cm^{-3}, the FF and PCE values drop. The increased doping levels result a built-in electric field (V_{bi}) [33]. This V_{bi} causes better separation of charge carriers towards their respective electrodes, thereby improving Voc. In the present study, the highest PCE value has been achieved for N_A as 10^{16} cm^{-3}; therefore, 10^{16} cm^{-3} is considered for further device optimization.

The number of defects (N_t) present in the active absorber layer defines the device performance. Therefore, the understanding of defects is

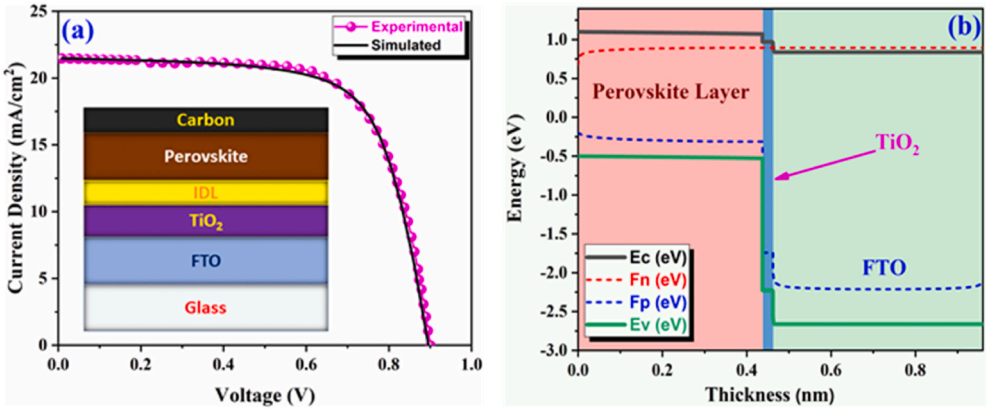

Fig. 2. (a) J-V characteristics of experimental and simulated results, inset shows the device configuration (b) energy level diagram of simulated results demonstrating perovskite, TiO_2 and FTO layers.

Table 2
Comparison between J-V parameters of simulated and experimental devices.

Work Mode	Jsc (mA/cm^2)	Voc (V)	FF (%)	PCE (%)	R_S (Ωcm^2)	R_{SH} (Ωcm^2)	Ref.
Experimental	21.45 ± 0.65	0.9 ± 0.2	69 ± 0.1	13.39 ± 0.3	–	–	[24]
Simulation	21.45	0.8953	69.06	13.26	2.35	1.0×10^{30}	This work

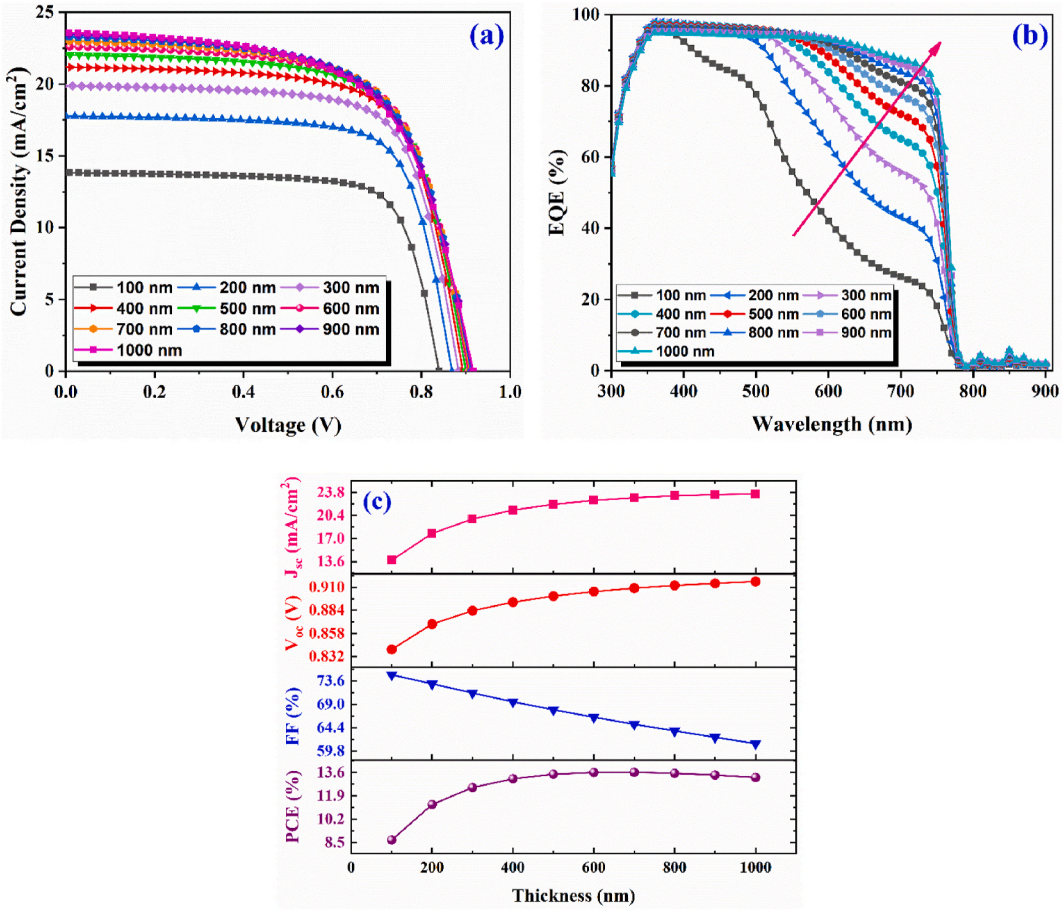

Fig. 3. Impact of variation in absorber layer thickness on (a) J-V curves (b) EQE curves (c) J- V parameters.

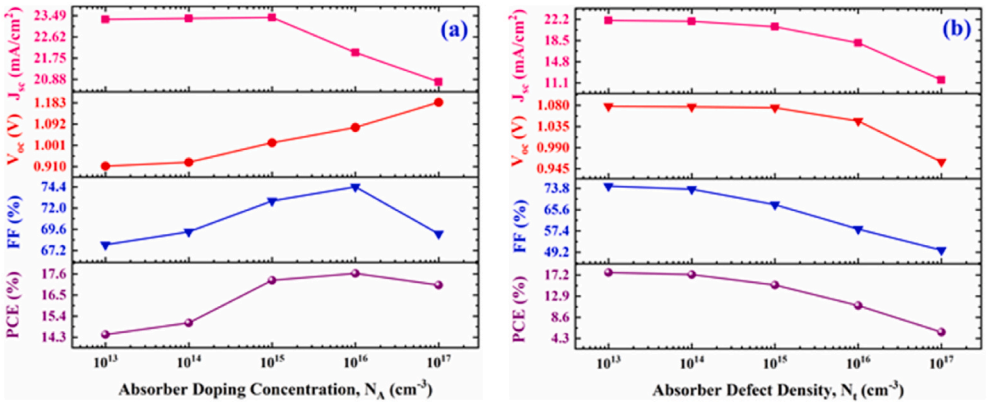

Fig. 4. (a) J-V parameters with varying absorber doping concentration (N_A) (b) absorber defect density (N_t) variation effect on J-V parameters.

essential to develop and analyze the highly efficient PSC. Here, the value of N_t is varied from 10^{13} to 10^{17} cm^{-3}, and the variation in device parameters is plotted in Fig. 4b. Results show that J-V parameters remain unchanged up to 10^{14} cm^{-3} and decrease as the N_t value increases. The Jsc drops from 21.87 to 11.63 mA/cm^2 as the N_t increases beyond 10^{14} cm^{-3}. The decrease in Jsc is attributed to higher number of trap states and thereby recombination mechanism with increased N_t values that causes losses in generated charge carriers [34]. Similarly, the Voc

decreases from 1.08 to 0.96 V. The FF, and PCE values degrade from 73.47 to 50.01% and 17.3 to 5.59%, respectively. This behavior could be described by the relation between N_t and the charge carriers (electron, hole) diffusion length (Ln, Lp), as explained by (1):

$$L_{n,\,p} = \sqrt{\frac{\mu_{n,\,p}\,kT}{q}\,\frac{1}{\sigma_{n,\,p}V_{th}N_t}} \tag{1}$$

Equ. 1 explains that $L_{n,\,p}$ is inversely proportional to N_t. Low N_t results in longer diffusion lengths, causes low recombination, and improves device performance. In contrast, the higher Nt causes shorter diffusion lengths, resulting in higher recombination and causes device performance degradation. In Table 3, the varying N_t values effect and the corresponding change in $L_{n,\,p}$ is demonstrated. The results are satisfying Equ. 1. In the present work, the N_t value is set as 2.6×10^{13} cm^{-3}, that leads to $L_{n,\,p}$ as 1.00 μm, as reported experimentally [35].

3.4. TiO_2 thickness and doping variation effect

The electron transport layer (ETL) is an important component of the PSC that allows the transmission of electrons and blockade of holes. TiO_2 is an n-type material widely used in HTL-free PSCs, and its thickness significantly affects the device performance [23]. To analyze the effect on HTL-free c-PSC structure, the ETL (TiO_2) thickness is varied from 10 to 100 nm, and obtained results are presented in Fig. 5a. Results reveal that Jsc, Voc, and PCE values decrease as the thickness of TiO_2 increases. In contrast, there is no considerable change in FF as it varies from 74.36 to 74.56 with increasing TiO_2 thickness from 10 to 100 nm. The reduction in performance of simulated device structure with increasing TiO_2 thickness is due to the lower transmittance in the wavelength range of 300–360 nm, as shown in Fig. S2. Also, the thick TiO_2 layer absorbs the incident light significantly and reduces the charge generation, hence decreases Jsc and PCE [36]. The thinner TiO_2 layer could not be a considerable choice as it could cause poor reproducibility. Similarly, the thinner layers may lead to recombination at the perovskite/FTO interface resulting in the leakage current. In addition, a thicker TiO_2 layer affects the device performance by reducing the Jsc, Voc, and hence PCE, as depicted in Fig. 5a. Therefore, we considered a 20 nm thick TiO_2 layer for further device performance optimization in the present study. This 20 nm thickness is in accordance with the experimentally reported value [37,38].

The TiO_2 donor doping density (N_D) effect on J-V parameters was analyzed by varying the doping concentration from 10^{13} to 10^{21} cm^{-3}. The obtained results are drawn in Fig. 5b. Our results exhibit that with increasing the N_D values, there is no change in J-V parameters. All parameters remain constant from 10^{13} to 10^{18} cm^{-3}. However, over 10^{18} cm^{-3}, the Jsc and Voc reduce and then saturate up to 10^{21} cm^{-3}. Similarly, the FF and PCE values follow an increasing pattern and remain stable up to 10^{21} cm^{-3}. In the present work, we considered 1.0×10^{20} cm^{-3} for further device performance optimization.

3.5. FTO thickness and doping variation effect

The impact of FTO thickness variation on HTL-free c-PSC performance is essential. The variation in J-V parameters with FTO thickness ranging from 100 to 1000 nm is shown in Fig. 6a. From the results, Jsc, Voc, and PCE values initially grow, after which they saturate and then start decreasing. Whereas the FF initially decreases and then follows an increasing pattern. With less thickness (<300 nm) of FTO, more light is transmitted to the absorber layer. With the absorbance of more light by the active layer, more charge carriers are generated, resulting in the increased current generation and consequently high Jsc. In contrast, beyond the 300 nm thickness of the FTO layer, the incident light is absorbed by the FTO that causes internal scattering and lengthening the direction of light [39]. Increased absorption by the FTO reduces the number of photons approaching the absorber layer, thus, reducing the generated current and, as a result, lowering the Jsc.

Results show that the Voc remains constant with increasing the FTO thickness. This is because the charge excitation, a primary process in PV, occurs in the absorber layer. Also, the absorber layer fermi level splitting is within the FTO band edges, hence causes constant Voc. As the FTO thickness increases from 100 to 1000 nm, the results show a minimal enhancement in FF from 74.31 to 74.67%. PCE, on the other hand, decreases as FTO thickness increases. As previously stated, a drop in efficiency is linked to a decrease in Jsc. Charge extraction can also be used to explain the reduction in Jsc. To be extracted through the FTO, the generated charges must have a longer lifetime, which is impossible. The increase in diffusion length causes increased charge recombination at the FTO and the TiO_2/FTO interface. The simulation results suggest that the FTO with 300 nm thickness will enhance the HTL-free c-PSC performance significantly.

In the present study, the donor doping concentration (N_D) of the FTO layer has been changed from 10^{13} to 10^{21} $cm^{-3,}$ and obtained results are plotted in Fig. 6b. The results demonstrate that the values of Jsc, Voc, and PCE initially increase slowly up to 10^{15} cm^{-3}. Beyond this point, these values increase linearly up to 10^{17} cm^{-3} and then saturates. The reverse saturation current decreases as the doping density increases, resulting in an increase in the Voc and, as a result, the PCE. The FF starts to increase up to 10^{15} cm^{-3}, from where it decreases with increasing doping concentration up to 10^{17} cm^{-3}. Beyond 10^{17} cm^{-3} doping value, the FF becomes constant, and no further change is observed, as depicted in Fig. 6b. In this work, we have set 1.0×10^{19} cm^{-3} as the FTO doping level value for further device performance optimization.

3.6. Interface (Perovskite/TiO_2) defect density variation effect

The interface quality is of particular importance towards the highly efficient solar cell. The reports show that, compared to the back interface, the interface defect density (N_t) close to the illuminated path significantly influences solar cell performance [27,40]. Thus, in the present study, the impact of N_t at TiO_2/perovskite interface on the PV performance of the designed solar cell is examined. The N_t values have been varied from 10^{13} to 10^{21} $cm^{-3,}$ and obtained results are depicted in Fig. 7. The results reveal that for N_t value below 10^{14} cm^{-3}, there is no change in device performance. The Jsc remains constant up to 10^{17} cm^{-3}; after that, it reduces, and beyond 10^{19} cm^{-3} it shows constant behavior. Similarly, the Voc remains constant up to 10^{15} cm^{-3}; after that, it falls, and then beyond 10^{19} cm^{-3} it follows the same trend as Jsc. The FF and PCE are severely influenced when the N_t increases over 10^{14} cm^{-3}. The decrease in the device PCE is correlated with increased Nt values, resulting in a high charge carrier recombination rate at the perovskite/TiO_2 interface [41]. Therefore, the N_t is selected at 1×10^{13} cm^{-3} to achieve highly efficient HTL-free c-PSCs.

3.7. Effect of variation in temperature and metal work function

The operating temperature is a significant factor towards the solar cells performance. Typically, solar panels operate over a temperature of 300 K. Therefore, the operating temperature effect on the HTL-free c-PSC performance is analyzed under a temperature range of 300–700 K. Fig. 8a shows the obtained J-V parameters with temperature variation. Results show that Jsc increases while Voc, FF, and PCE reduce with rising temperature. The growing trend in Jsc with increasing

Table 3
Variation in the diffusion lengths of electron and hole with defect density (N_t).

Defect Density, Nt (cm^{-3})	1×10^{13}	1×10^{14}	1×10^{15}	1×10^{16}	1×10^{17}
Hole Diffusion Length Lp (μm)	1.6	0.51	0.16	0.051	0.016
Electron Diffusion Length Ln (μm)	1.6	0.51	0.16	0.051	0.016

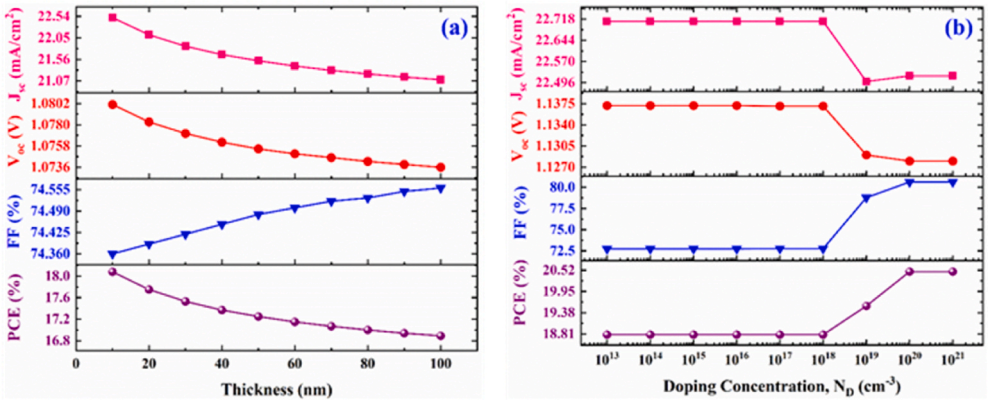

Fig. 5. The effect on J-V parameters with (a) variation in TiO_2 thickness (b) variation in TiO_2 doping concentration.

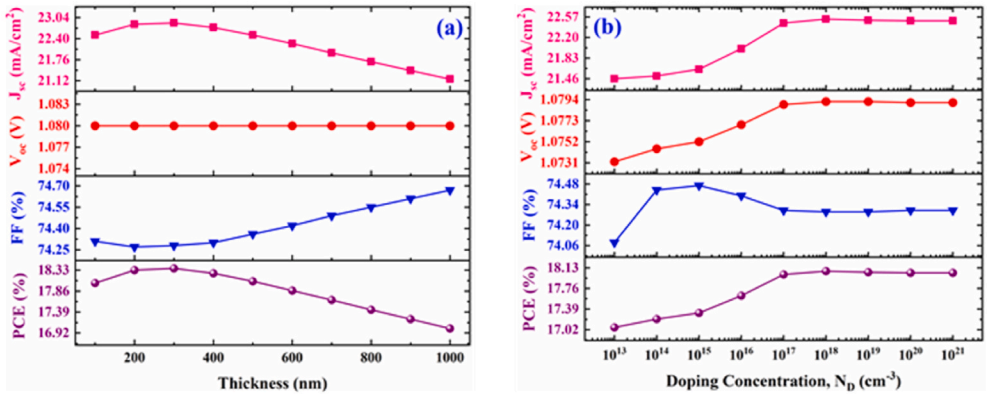

Fig. 6. The effect on J-V parameters with (a) variation in FTO thickness (b) variation in FTO doping concentration.

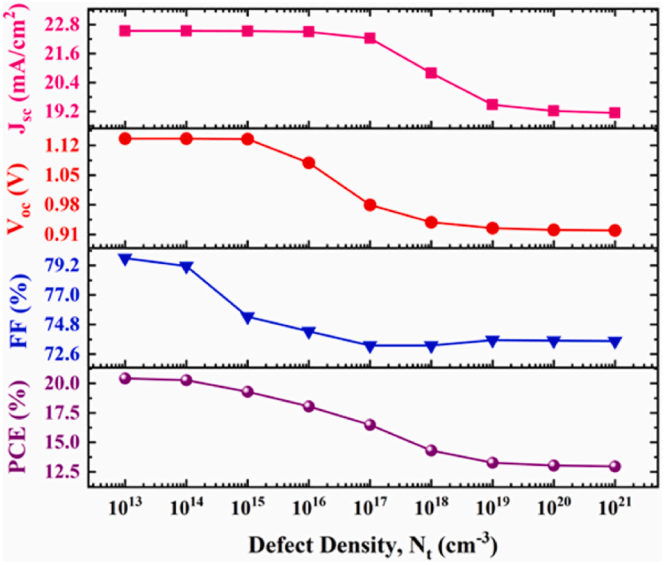

Fig. 7. Interface defect density (N_t) effect on J-V parameters.

temperature is attributed to the reduction in the energy bandgap that leads to the generation of additional charge carriers and consequently increased Jsc [42]. Similarly, the drop in Voc can be clarified by forming interfacial defects, including increased series resistance and reduction in carrier diffusion length [42]. The reduced pattern of Voc results in degradation of the overall device performance. Table 4 shows a comparison between the obtained simulated and experimentally reported results at 673.15 K [29]. The results show that the simulated and experimentally reported data are in decent agreement and validate our simulated model.

Fig. 8b depicts the device performance as the work function of the back metal contact varies from 4.6 to 5.7 eV. This range of work functions is for different metal contacts such as silver (Ag), iron (Fe), carbon (C), gold (Au), nickel (Ni), and platinum (Pt). The associated work functions of these metals are mentioned in Table 5. Results reveal that all parameters improve with increasing back metal work function. As metal work function increases, the barrier height of the majority carriers (concerning fermi level energy) lowers because of band bending at the metal-semiconductor interface, resulting in more ohmic contact [43]. With increasing the work function, the Voc increases sharply. Hence, the increase in Voc leads to improvement in PCE of HTL-free c-PSC. From the results, excellent performance is achieved for Pt (5.7 eV). However, the increased cost related to Pt may limit its application towards cost-effective HTL-free c-PSCs. Therefore, C (5.0 eV) can be used as an adequate substitute for expensive metal electrodes.

The results also show that an efficiency of 20.43% can be obtained using the FTO/TiO_2/Perovskite/C for cost-effective and efficient HTL-free PSCs.

In Table 6, a detailed comparison of our simulated results with already reported experiment results is summarized. Our simulated results show a substantial improvement in overall device performance. The Jsc and FF values in our simulated work are in well agreement with the experimental reported work [44]. In addition, the step-by-step optimization from initial to the final optimized values, including the absorber, TiO_2, FTO thicknesses, and doping variations, is presented in Fig. S3. The J-V parameters are also given in Table S1.

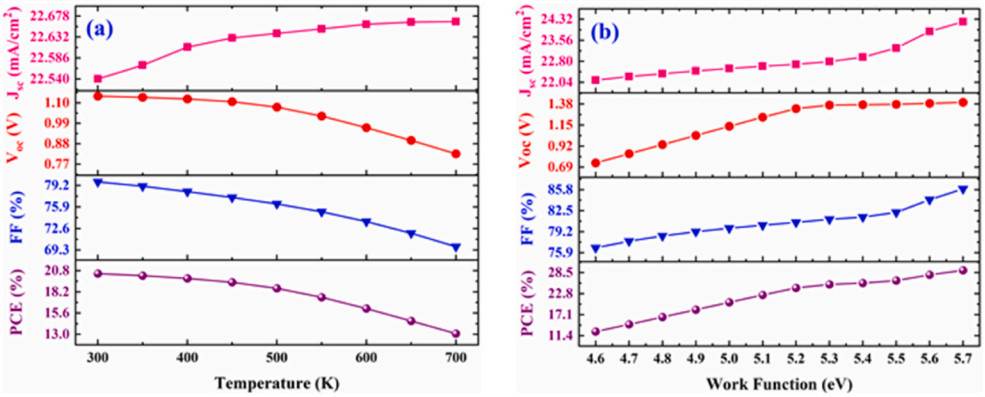

Fig. 8. (a) Temperature effect on J-V parameters (b) work function variation effect on J-V parameters.

Table 4
Comparison of simulated and experimental reported results (400 °C = 673.15 K).

Working Mode	Temperature	Jsc (mA/cm^2)	Voc (V)	FF (%)	PCE (%)	Ref.
Experimental	400 °C	21.45 ± 0.65	0.9 ± 0.2	69 ± 0.1	13.39 ± 0.3	[24]
Simulated	673.15 K	22.66	0.86	70.94	13.91	This work

Table 5
Detail of work functions of different back metal contacts.

Metal Contacts	Silver (Ag)	Iron (Fe)	Carbon (C)	Gold (Au)	Nickel (Ni)	Platinum (Pt)
Work Function (eV)	4.74	4.81	5	5.1	5.5	5.70

Table 6
Comparison of different HTL-free PSC structures J-V parameters of experimental and simulated work.

S. No.	Working Mode	Jsc (mA/cm^2)	Voc (V)	FF (%)	PCE (%)	Ref.
1	Experiment	21.45 ± 0.65	0.9 ± 0.2	69 ± 0.1	13.39 ± 0.3	[24]
2		22.69	0.9	79	16.21	[44]
3	Simulation	22.30	1.06	60.36	14.27	[25]
4		22.32	0.96	80.22	17.21	[45]
5		22.54	1.13	79.75	20.43	This work

4. Conclusion

To conclude, the device modeling of $Cs_x(FA_{0.4}MA_{0.6})_{1-x}PbI_{2.8}Br_{0.2}$ based HTL-free c-PSC was carried out using SCAPS. Initially, the modeling was verified with the experimental results and found to be in decent agreement. Several elements that can affect device performance were thoroughly investigated. Simulation results suggest the optimized thicknesses of the $Cs_x(FA_{0.4}MA_{0.6})_{1-x}PbI_{2.8}Br_{0.2}$, TiO_2 and FTO are 800 nm, 20 nm, and 300 nm, respectively. Similarly, 1.0×10^{16} cm^{-3}, 1.0×10^{20} cm^{-3} and 1.0×10^{19} cm^{-3} doping concentrations for $Cs_x(FA_{0.4}MA_{0.6})_{1-x}PbI_{2.8}Br_{0.2}$, TiO_2 and FTO, respectively, exhibited enhanced device performance. The optimal defect density value as 2.60×10^{13} cm^{-3} for the absorber is consistent with the experimental data. The results also propose that the IDL at the perovskite/TiO_2 interface should be minimum to achieve high-performance HTL-free c-PSC. Therefore, the 1.0×10^{13} cm^{-3} is the optimized value of IDL. These optimal values enhanced our experimentally reported HTL-free c-PSC PCE from 13.39% to over 20%. In addition, the temperature effect and back metal contact work function were also studied. The results demonstrate that a 300 K operating temperature is ideal for achieving high efficiency of HTL-free c-PSC. Also, platinum with a work function of 5.7 eV was found as a highly efficient back metal contact material. However, we considered carbon a low-cost and stable back metal contact layer for stable and cost-effective HTL-free c-PSC. Based on optimized results, the highest Voc, Jsc, FF, and PCE values are observed as 1.13 V, 22.54 mA/cm^2, 79.75%, and 20.43%, respectively. Finally, the present study indicates the future directions for an efficient, simple, stable, and cost-effective HTL-free $Cs_x(FA_{0.4}MA_{0.6})_{1-x}PbI_{2.8}Br_{0.2}$ based c-PSCs.

CRediT authorship contribution statement

Ehsan Raza: Methodology, Data curation, Writing – original draft, preparation. **Zubair Ahmad:** Conceptualization, Methodology, Supervision, Validation, Writing – review & editing. **Muhammad Asif:** Writing – review & editing. **Fakhra Aziz:** Writing – review & editing. **Kashif Riaz:** Writing – review & editing. **Muhammad Qasim Mehmood:** Writing – review & editing. **Jolly Bhadra:** Writing – review & editing, and. **Noora J. Al-Thani:** Writing – review & editing.

Declaration of competing interest

The authors declare that they have no known competing financial interests or personal relationships that could have appeared to influence the work reported in this paper.

Acknowledgments

This publication was made possible by NPRP grant # NPRP11S-1210–170080 from the Qatar National Research Fund (a member of Qatar Foundation). The findings achieved herein are solely the responsibility of the authors. We are also thankful to Prof. Marc Burgelman at the University of Gent in Belgium for providing us access to the SCAPS software.

Appendix A. Supplementary data

Supplementary data to this article can be found online at https://doi.org/10.1016/j.optmat.2022.112075.

References

[1] N. Li, Z. Zhu, J. Li, A.K.Y. Jen, L. Wang, Inorganic CsPb1− xSnxIBr2 for efficient wide-bandgap perovskite solar cells, Adv. Energy Mater. 8 (2018) 1800525.

[2] Q. Ou, X. Bao, Y. Zhang, H. Shao, G. Xing, X. Li, L. Shao, Q. Bao, Band structure engineering in metal halide perovskite nanostructures for optoelectronic applications, Nano Mater. Sci. 1 (2019) 268–287.

[3] F. Zhang, B. Yang, Y. Li, W. Deng, R. He, Extra long electron–hole diffusion lengths in CH 3 NH 3 PbI 3− x Cl x perovskite single crystals, J. Mater. Chem. C 5 (2017) 8431–8435.

[4] L.M. Herz, Charge-carrier mobilities in metal halide perovskites: fundamental mechanisms and limits, ACS Energy Lett. 2 (2017) 1539–1548.

[5] A. Kojima, K. Teshima, Y. Shirai, T. Miyasaka, Organometal halide perovskites as visible-light sensitizers for photovoltaic cells, J. Am. Chem. Soc. 131 (2009) 6050–6051.

[6] NREL. https://www.nrel.gov/pv/cell-efficiency.html, 2020.

[7] L. Zhang, C. Liu, J. Zhang, X. Li, C. Cheng, Y. Tian, A.K.Y. Jen, B. Xu, Intensive exposure of functional rings of a polymeric hole-transporting material enables efficient perovskite solar cells, Adv. Mater. 30 (2018) 1804028.

[8] H. Zou, D. Guo, B. He, J. Yu, K. Fan, Enhanced photocurrent density of HTM-free perovskite solar cells by carbon quantum dots, Appl. Surf. Sci. 430 (2018) 625–631.

[9] Q. Wali, F.J. Iftikhar, M.E. Khan, A. Ullah, Y. Iqbal, R. Jose, Advances in stability of perovskite solar cells, Org. Electron. 78 (2020) 105590.

[10] M.M. Lee, J. Teuscher, T. Miyasaka, T.N. Murakami, H.J. Snaith, Efficient hybrid solar cells based on meso-superstructured organometal halide perovskites, Science 338 (2012) 643–647.

[11] M. Liu, M.B. Johnston, H.J. Snaith, Efficient planar heterojunction perovskite solar cells by vapour deposition, Nature 501 (2013) 395–398.

[12] A. Mei, X. Li, L. Liu, Z. Ku, T. Liu, Y. Rong, M. Xu, M. Hu, J. Chen, Y. Yang, A hole-conductor–free, fully printable mesoscopic perovskite solar cell with high stability, Science 345 (2014) 295–298.

[13] C. Huang, P. Lin, N. Fu, C. Liu, B. Xu, K. Sun, D. Wang, X. Zeng, S. Ke, Facile fabrication of highly efficient ETL-free perovskite solar cells with 20% efficiency by defect passivation and interface engineering, Chem. Commun. 55 (2019) 2777–2780.

[14] S. Liu, W. Huang, P. Liao, N. Pootrakulchote, H. Li, J. Lu, J. Li, F. Huang, X. Shai, X. Zhao, 17% efficient printable mesoscopic PIN metal oxide framework perovskite solar cells using cesium-containing triple cation perovskite, J. Mater. Chem. 5 (2017) 22952–22958.

[15] R. Taheri-Ledari, K. Valadi, A. Maleki, High-performance HTL-free perovskite solar cell: an efficient composition of ZnO NRs, RGO, and CuInS2 QDs, as electron-transporting layer matrix, Prog. Photovoltaics Res. Appl. 28 (2020) 956–970.

[16] Y. Zhang, X. Hu, L. Chen, Z. Huang, Q. Fu, Y. Liu, L. Zhang, Y. Chen, Flexible, hole transporting layer-free and stable CH3NH3PbI3/PC61BM planar heterojunction perovskite solar cells, Org. Electron. 30 (2016) 281–288.

[17] S. Ye, H. Rao, Z. Zhao, L. Zhang, H. Bao, W. Sun, Y. Li, F. Gu, J. Wang, Z. Liu, A breakthrough efficiency of 19.9% obtained in inverted perovskite solar cells by using an efficient trap state passivator Cu (thiourea) I, J. Am. Chem. Soc. 139 (2017) 7504–7512.

[18] W.-Q. Wu, Q. Wang, Y. Fang, Y. Shao, S. Tang, Y. Deng, H. Lu, Y. Liu, T. Li, Z. Yang, Molecular doping enabled scalable blading of efficient hole-transport-layer-free perovskite solar cells, Nat. Commun. 9 (2018) 1–8.

[19] D. Bogachuk, S. Zouhair, K. Wojciechowski, B. Yang, V. Babu, L. Wagner, B. Xu, J. Lim, S. Mastroianni, H. Pettersson, Low-temperature carbon-based electrodes in perovskite solar cells, Energy Environ. Sci. 13 (2020) 3880–3916.

[20] Z. Ku, Y. Rong, M. Xu, T. Liu, H. Han, Full printable processed mesoscopic CH 3 NH 3 PbI 3/TiO 2 heterojunction solar cells with carbon counter electrode, Sci. Rep. 3 (2013) 1–5.

[21] H. Zhang, H. Wang, S.T. Williams, D. Xiong, W. Zhang, C.C. Chueh, W. Chen, A.K. Y. Jen, SrCl2 derived perovskite facilitating a high efficiency of 16% in hole-conductor-free fully printable mesoscopic perovskite solar cells, Adv. Mater. 29 (2017) 1606608.

[22] S. Wang, Y. Jiang, E.J. Juarez-Perez, L.K. Ono, Y. Qi, Accelerated degradation of methylammonium lead iodide perovskites induced by exposure to iodine vapour, Nat. Energy 2 (2016) 1–8.

[23] S.M. Meroni, C. Worsley, D. Raptis, T.M. Watson, Triple-Mesoscopic carbon perovskite solar cells: materials, processing and applications, Energies 14 (2021) 386.

[24] Z. Ahmad, A. Mishra, S.M. Abdulrahim, F. Touati, Electrical equivalent circuit (EEC) based impedance spectroscopy analysis of HTM free perovskite solar cells, J. Electroanal. Chem. 871 (2020) 114294.

[25] S. Rai, B. Pandey, D. Dwivedi, Device simulation of low cost HTM free perovskite solar cell based on TiO2 electron transport layer, in: AIP Conference Proceedings, AIP Publishing LLC, 2020, p. 140022.

[26] L. Lin, P. Li, Z. Kang, H. Xiong, Y. Chen, Q. Yan, L. Jiang, Y. Qiu, Device design of doping-controlled homojunction perovskite solar cells omitting HTL and exceeding 25% efficiency, Adv. Theor. Simul. 4 (2021) 2000222.

[27] L. Lin, P. Li, L. Jiang, Z. Kang, Q. Yan, H. Xiong, S. Lien, P. Zhang, Y. Qiu, Boosting efficiency up to 25% for HTL-free carbon-based perovskite solar cells by gradient doping using SCAPS simulation, Sol. Energy 215 (2021) 328–334.

[28] M. Burgelman, P. Nollet, S. Degrave, Modelling polycrystalline semiconductor solar cells, Thin Solid Films 361 (2000) 527–532.

[29] A. Mishra, Z. Ahmad, I. Zimmermann, D. Martineau, R. Shakoor, F. Touati, K. Riaz, S.A. Al-Muhtaseb, M.K. Nazeeruddin, Effect of annealing temperature on the performance of printable carbon electrodes for perovskite solar cells, Org. Electron. 65 (2019) 375–380.

[30] E. Raza, Z. Ahmad, F. Aziz, M. Asif, A. Ahmed, K. Riaz, J. Bhadra, N.J. Al-Thani, Numerical simulation analysis towards the effect of charge transport layers electrical properties on cesium based ternary cation perovskite solar cells performance, Sol. Energy 225 (2021) 842–850.

[31] T. Minemoto, Y. Kawano, T. Nishimura, J. Chantana, Numerical reproduction of a perovskite solar cell by device simulation considering band gap grading, Opt. Mater. 92 (2019) 60–66.

[32] L. Lin, L. Jiang, Y. Qiu, Y. Yu, Modeling and analysis of HTM-free perovskite solar cells based on ZnO electron transport layer, Superlattice. Microst. 104 (2017) 167–177.

[33] A. Bag, R. Radhakrishnan, R. Nekovei, R. Jeyakumar, Effect of absorber layer, hole transport layer thicknesses, and its doping density on the performance of perovskite solar cells by device simulation, Sol. Energy 196 (2020) 177–182.

[34] H.K. Ibrahim, A.M. Sabaawi, Q.T. Algwari, Study of defects in CH3NH3PbI3-based perovskite solar cells, in: IOP Conference Series: Materials Science and Engineering, IOP Publishing, 2021, p. 12032.

[35] S.D. Stranks, G.E. Eperon, G. Grancini, C. Menelaou, M.J. Alcocer, T. Leijtens, L. M. Herz, A. Petrozza, H.J. Snaith, Electron-hole diffusion lengths exceeding 1 micrometer in an organometal trihalide perovskite absorber, Science 342 (2013) 341–344.

[36] Y. Raoui, H. Ez-Zahraouy, N. Tahiri, O. El Bounagui, S. Ahmad, S. Kazim, Performance analysis of MAPbI3 based perovskite solar cells employing diverse charge selective contacts: simulation study, Sol. Energy 193 (2019) 948–955.

[37] A. Sławek, Z. Starowicz, M. Lipiński, The influence of the thickness of compact TiO2 electron transport layer on the performance of planar CH3NH3PbI3 perovskite solar cells, Materials 14 (2021) 3295.

[38] G. Mathiazhagan, L. Wagner, S. Bogati, K.b.Y. Ünal, D. Bogachuk, T. Kroyer, S. Mastroianni, A. Hinsch, Double-mesoscopic hole-transport-material-free perovskite solar cells: overcoming charge-transport limitation by sputtered ultrathin Al2O3 isolating layer, ACS Appl. Nano Mater. 3 (2020) 2463–2471.

[39] W. Isoe, M. Mageto, C. Maghanga, M. Mwamburi, V. Odari, C. Awino, Thickness dependence of window layer on CH3NH3PbI3-XClX perovskite solar cell, Int. J. Photoenergy (2020) 2020.

[40] L. Huang, X. Sun, C. Li, R. Xu, J. Xu, Y. Du, Y. Wu, J. Ni, H. Cai, J. Li, Electron transport layer-free planar perovskite solar cells: further performance enhancement perspective from device simulation, Sol. Energy Mater. Sol. Cell. 157 (2016) 1038–1047.

[41] T. Minemoto, M. Murata, Device modeling of perovskite solar cells based on structural similarity with thin film inorganic semiconductor solar cells, J. Appl. Phys. 116 (2014) 54505.

[42] T. Ouslimane, L. Et-Taya, L. Elmaimouni, A. Benami, Impact of absorber layer thickness, defect density, and operating temperature on the performance of MAPbI3 solar cells based on ZnO electron transporting material, Heliyon 7 (2021) e06379.

[43] F. Behrouznejad, S. Shahbazi, N. Taghavinia, H.-P. Wu, E.W.-G. Diau, A study on utilizing different metals as the back contact of CH 3 NH 3 PbI 3 perovskite solar cells, J. Mater. Chem. 4 (2016) 13488–13498.

[44] Q. Wang, W. Zhang, Z. Zhang, S. Liu, J. Wu, Y. Guan, A. Mei, Y. Rong, Y. Hu, H. Han, Crystallization control of ternary-cation perovskite absorber in triple-mesoscopic layer for efficient solar cells, Adv. Energy Mater. 10 (2020) 1903092.

[45] D. Pal, S. Das, Numerical modeling and simulation for augmenting the photovoltaic response of HTL free perovskite solar cells, Mater. Today Proc. 46 (2021) 6367–6373.